Available online at www.sciencedirect.com
ScienceDirect
Trans. Nonferrous Met. Soc. China 35(2025) 1822−1836
Transactions of Nonferrous Metals Society of China
www.tnmsc.cn

Friction and wear performance of fluorinated Ti48Al2Nb2Cr alloy

Ji-jian GUO, Zhe-xuan LI, Qing-qing SUN, Lian-kui WU, Fa-he CAO

School of Materials, Sun Yat-sen University, Shenzhen 518107, China

Received 23 October 2023; accepted 22 March 2024

Abstract: To improve the friction and wear performance at room and elevated temperatures, Ti48Al2Nb2Cr (at.%) alloy was anodically fluorinated in an NH_4F-containing electrolyte. The effects of anodic fluorination on the friction coefficient, wear rate, wear track morphology, and adhesion strength between the oxide scale and substrate were investigated. Results showed that the in-situ formation of Al_2O_3-enriched oxide scale was promoted due to fluorine effect, by which the surface hardness and wear resistance were both enhanced. After the friction and wear test, no noticeable changes were found on the fluorinated Ti48Al2Nb2Cr, whilst severe abrasion was evident on the GCr15 counterpart. This indicates that anodic fluorination could effectively enhance the friction and wear performance of Ti48Al2Nb2Cr alloy. At elevated temperatures, the dominant wear mechanism of the fluorinated Ti48Al2Nb2Cr/GCr15 pair was oxidation wear and adhesive wear.

Key words: TiAl alloy; anodic fluorination; fluorine effect; tribological property; wear resistance

1 Introduction

TiAl alloys are promising candidates for compressor and low-pressure turbine blades, owing to their low density, high specific strength, and high temperature creep resistance [1−5]. The poor oxidation resistance and wear resistance, however, impede their further application. During the past several decades, most research efforts have been devoted to enhancing the oxidation resistance of TiAl alloys by alloying design [6−8], surface modification [9−12], and applying protective coating [13−16].

In the meantime, the research regarding the wear resistance of TiAl alloys has also gained considerable attention [17−22]. For instance, in a study on the wear behavior of Ti48Al2Nb2Cr (at.%) with nickel base superalloy at different temperatures from 296 to 823 K, MIYOSHI et al [17] reported a strong correlation between the wear performance and the service temperatures. MENGIS et al [19] found that the TiAl alloy exhibited the worst wear resistance at 400 °C due to the oxidation of Ti and Al. Recently, WU et al [23] have found that as the applied load increased, the friction coefficient and wear-scar volume of Ti48Al2Cr2Nb alloy decreased due to the combined effect of adhesive wear and oxidation wear.

Apart from the more fundamental studies on the wear behavior of TiAl alloys, a significant amount of efforts were dedicated to improving the wear resistance through various approaches. In this line of research, surface treatment is the most extensively studied, including thermal oxidation [24] or nitridation [25], plasma carburization [26], laser cladding [27], micro-arc oxidation [28], and application of coating [29]. LI et al [27] found that the laser-cladding Ti_3Al/TiAl + TiC ceramic layer could reduce the wear rate of TC4 alloy by two times. However, the large thermal stress generated during the laser cladding process made the Ti_3Al/

Corresponding author: Lian-kui WU, E-mail: wulk5@mail.sysu.edu.cn
https://doi.org/10.1016/S1003-6326(25)66785-9

TiAl + TiC ceramic coating easy to peel off from the substrate. WU et al [28] found that the introduction of sodium citrate, graphite, and sodium tungstate into the micro-arc electrolyte solution was able to improve the wear resistance of TiAl alloy due to the generation of WO_3, Ti_2O_3, and Al_2O_3. LI et al [29] prepared Mo−Si−Ti coating with composition and structure gradients to improve the wear resistance of γ-TiAl.

Recently, we have proposed to regulate the surface structure and composition of TiAl alloy by anodization in fluorine-containing electrolytes [10,11,30]. During thermal exposure to air, a protective Al_2O_3 layer will be in-situ generated on the fluorinated TiAl alloy due to the fluorine effect. Results showed that the oxidation resistance [10,11] and hot corrosion resistance [30] of the fluorinated TiAl alloy were efficiently improved. Moreover, owing to this Al_2O_3-enriched oxide layer, the friction and wear resistance of the fluorinated Ti45Al8.5Nb alloy was significantly enhanced at 1000 °C [22]. Although the close relationship between the tribological properties and service temperature has been identified in many studies, a fundamental understanding of how the service temperature affects friction and wear performance is still lacking. This requires the characterization of the friction and wear behavior not only on the pristine fluorinated TiAl alloys but also on the fluorinated samples at the service temperature in-situ.

In this vein of thought, the present work aimed to systematically study the friction and wear behavior of the fluorinated Ti48Al2Nb2Cr alloy both at room temperature and at high service temperature in-situ. The wear profiles of the specimens were characterized by 3D wide-field microscope. The micro-morphology of the wear profiles and debris was assessed by a scanning electron microscope (SEM) coupled with energy dispersive spectroscopy (EDS). The evolution of hardness was recorded. The adhesion of the oxide scale was evaluated by an automatic scratch instrument.

2 Experimental

2.1 Anodic fluorination

TiAl alloy with a nominal composition of Ti48Al2Cr2Nb (at.%) was cast by a vacuum furnace. Samples with the size of 15 mm × 15 mm × 1 mm were ground with sandpaper with the grit of 60# to remove the natural oxide scale, then ultrasonically cleaned in acetone and ethanol for 5 min sequentially, and finally rinsed with deionized water and anhydrous ethanol. The specimens were dried in warm air before the testing.

Using ethylene glycol containing 0.15 mol/L NH_4F as electrolyte, anodic fluorination was conducted at 5 V for 1 h [30]. Two graphite plates with an exposure area of 100 mm × 40 mm were used as the cathodes, and Ti48Al2Nb2Cr alloy was used as the anode. Ti48Al2Nb2Cr alloy was hung between two graphite plates with a distance of ~5 cm. The electrolyte was magnetically stirred during anodic fluorination. After anodic fluorination, the specimens were taken out from the electrolyte, ultrasonically cleaned in deionized water, and dried by warm air.

2.2 Measurements of tribological properties of specimens

The tribological properties of the fluorinated Ti48Al2Nb2Cr alloy were evaluated on an MDW−02G tribometer (Jinan Yihua, China) with a GCr15 steel ball (diameter d = 6 mm) as the counterpart ball. The tribological test was carried out in reciprocating sliding mode under dry conditions. Before the tribological test, the GCr15 steel balls were cleaned ultrasonically in ethanol for 10 min to remove the surface contamination. With a frequency of 1 Hz and a displacement amplitude of 12 mm, a normal load of 5 N was applied for 10 min. After the test, the specimen was ultrasonically cleaned in deionized water for 5 min and dried by warm air. The tribological property of the fluorinated Ti48Al2Al2Nb at room temperature was evaluated after the specimens were oxidized in a chamber furnace at 1000 °C for different durations (KSL−1200X, Hefei Kejing Co., Ltd., China). The wear loss of the specimens was calculated using the equation below:

$$\omega = V/(F \cdot L)$$

where ω is the wear rate ($mm^3/(N \cdot m)$), V is the wear volume (mm^3), F is the applied normal load (N), and L is the sliding distance (m).

2.3 Characterization of specimens

The phase composition of the specimen was analyzed by X-ray diffraction (Panalytical X'Pert

PRO, Cu K_α (λ=0.154056 nm, 40 kV, and 40 mA). The morphology and profile of the wear track were characterized by scanning electron microscope (SEM, Gemini500) and 3D wide-field microscope (DVM6M, Leica, Germany). The adhesion strength was tested by a scratch tester (WS−2005). A diamond indenter with a radius of 200 μm was employed to make a scratch on the coating at a continuously growing load in a range of 0−20 N. The micro Vickers hardness of the specimen was tested by an HMV-G21S (Shimadzu) instrument. The load was 9.8 N, and the holding time was 10 s. Three parallel tests were conducted under each condition.

3 Results and discussion

3.1 Tribological properties of fluorinated Ti48Al2Nb2Cr at room temperature

Figure 1 reveals the XRD patterns of the fluorinated Ti48Al2Nb2Cr after oxidation at 1000 °C for different time. TiAl and Ti_3Al come from the alloy substrate, while TiO_2 and Al_2O_3 are derived from the oxide scales. Notably, after thermal exposure to air, TiO_2 with strong diffraction intensity is observed on the untreated Ti48Al2Nb2Cr alloy [30], whilst the diffraction intensity is reduced on these fluorinated specimens (Fig. 1). This is due to the fluorine effect which promotes the formation of Al_2O_3 whilst restrains the formation of TiO_2 [10,11,31].

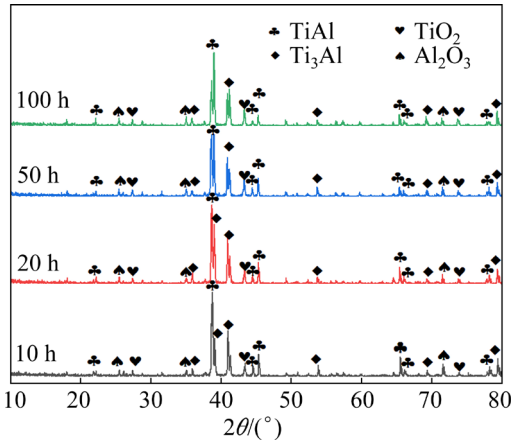

Fig. 1 XRD patterns of fluorinated Ti48Al2Nb2Cr after oxidation at 1000 °C for different time

The tribological properties of the fluorinated Ti48Al2Nb2Cr at room temperature were studied. As shown in Fig. 2, a relatively high friction coefficient (up to 0.7) is observed on the untreated Ti48Al2Nb2Cr alloy, consistent with that of GCr15/TiAlNb [32]. Interestingly, the friction coefficient was dramatically reduced after the anodic fluorination. For all fluorinated specimens, relatively low friction coefficients (~0.3) are found in comparison to the untreated alloy (up to 0.7), suggesting that the alumina and fluorine-enriched anodic film could induce a low friction regime, in line with the observations from WANG et al [33] and LEE et al [34]. They attributed this to the formation of an aluminum hydroxide layer with a crystallographic structure as a result of the tribo-chemical reaction between the anodic film and GCr15. LEE et al [34] suggested that this aluminum hydroxide layer could play a role as a lubricating layer. Moreover, it is found that the friction coefficient increases with the increase of the oxidation time. This observation can be ascribed to two factors. For one thing, lengthening the thermal exposure time to air prompts the generation of an oxide scale with enhanced surface roughness [11]. This would increase the real contact area between the specimen and the friction pair, therefore leading to a high friction coefficient. For another, the contact between the GCr15 counterpart and the fluorinated Ti48Al2Nb2Cr alloy results in serious adhesive wear because the Al_2O_3-enriched oxide scale on the fluorinated Ti48Al2Nb2Cr alloy has a high hardness feature and can destroy the GCr15 counterpart. The derived wear debris from the GCr15 counterpart would lead to abrasive wear, therefore increasing the friction coefficient.

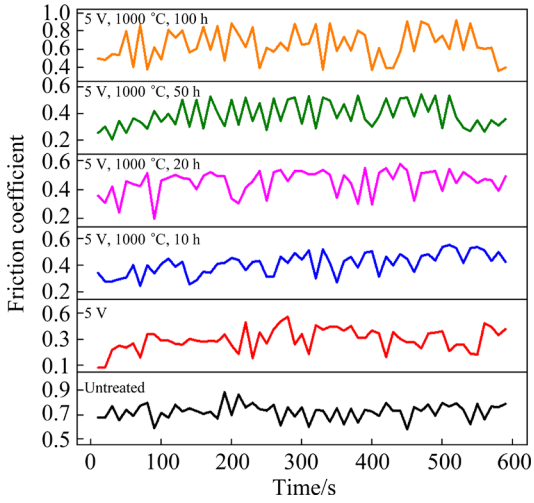

Fig. 2 Friction coefficients as function of testing time at 25 °C for untreated and fluorinated Ti48Al2Nb2Cr after oxidation at 1000 °C for different time

The 2D morphology and 3D topography images of the wear tracks for untreated and fluorinated Ti48Al2Nb2Cr were collected after the room temperature tribological test (Fig. 3). The deep wear scratches and distributed debris on the wear tracks demonstrate that both untreated (Figs. 3(a_1, a_2)) and fluorinated Ti48Al2Nb2Cr (Figs. 3(b_1−f_1, b_2−f_2)) suffer from severe wear. The obvious plow grooves in the wear tracks suggest that the abrasive wear occurs on the two specimens.

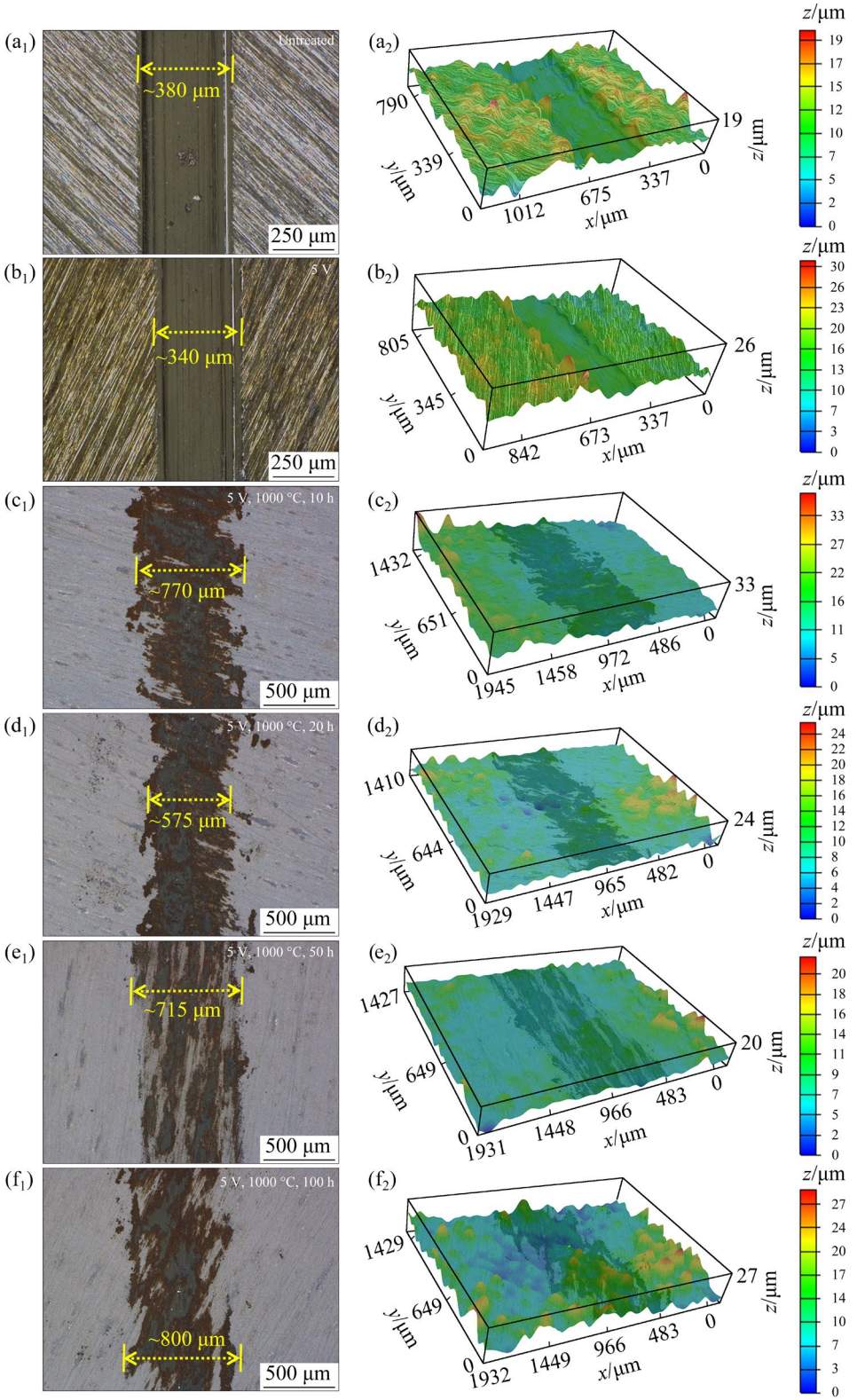

Fig. 3 2D (a_1−f_1) and 3D (a_2−f_2) topography images of wear tracks for untreated (a_1, a_2) and fluorinated (b_1−f_1, b_2−f_2) Ti48Al2Nb2Cr after oxidation at 1000 °C for different time

After oxidation at 1000 °C (Figs. 3(c_1−f_1, c_2−f_2)), although obvious wear tracks are still observed on the fluorinated Ti48Al2Nb2Cr, the oxide scales are not worn out. In addition, red-brown products from the adhesion wear of GCr15 counterparts are found. These suggest that the contact between the Al_2O_3-dominated oxide scale and the GCr15 counterpart leads to severe abrasion for the latter. The formation of an Al_2O_3-enriched oxide scale on the fluorinated specimen is induced as a result of the fluorine effect [10,11,31]. The top surface morphology (Figs. 3(a_1−f_1)) and 3D topography images (Figs. 3(a_2−f_2)) also reveal that the width of the wear tracks increases with the increase of the thermal oxidation duration, suggesting an enhanced wear resistance owing to the Al_2O_3 dominant oxide scale.

Figure 4 shows the top-surface SEM images and corresponding EDS mappings of the wear tracks of untreated and fluorinated Ti48Al2Nb2Cr after oxidation at 1000 °C. Clear boundaries and deep grooves, the typical characteristics of abrasive wear, are observed on both untreated (Fig. 4(a)) and fluorinated (Fig. 4(c)) Ti48Al2Nb2Cr. EDS analysis indicates that the wear tracks for both specimens have similar compositions with the alloy matrix (Points 2 and 4, Table 1 and Fig. 4). For the fluorinated specimens oxidized for different durations, all wear tracks are discontinuous and no clear track boundaries can be found (Figs. 4(e−l)). Furthermore, EDS analysis indicates that Fe element, the main component of the GCr15 counterpart, dominates these wear tracks (Table 1 and Figs. 4(f, h, j, l). The Al_2O_3-enriched oxide scale has a higher hardness than that of the GCr15 counterpart, resulting in the abrasion of the GCr15 counterpart. The wear mechanism of these specimens is assigned to adhesion wear and oxidation wear. In addition, it is found that the Al content of the oxide scale increases with the prolonging of oxidation time and reaches 32.2 at.% after 100 h oxidation (Point 11, Fig. 4(k) and Table 1). Meanwhile, this specimen exhibits excellent wear resistance.

To further study the influence of anodic fluorination on the friction and wear properties of Ti48Al2Nb2Cr, the wear rate of the specimens was calculated. The results show that the wear rate of the fluorinated Ti48Al2Nb2Cr is much lower than that of the untreated Ti48Al2Nb2Cr (Fig. 5), consistent with the evolution rule of friction coefficients as shown in Fig. 2. This may be attributed to the lubrication effect caused by the product generated due to the tribo-chemical reaction between the anodic film and the GCr15 counterpart [34]. In addition, the wear rate decreases with the prolonging of thermal exposure time, and negative values are obtained when the oxidation time exceeds 10 h. This indicates that the specimens are not abrased but rather the abrasive particles transferred from the GCr15 counterpart accumulate on the alloy due to the adhesive wear. The wear rate results presented in Fig. 5 indicate that the wear resistance is gradually improved with the lengthening of thermal exposure time.

3.2 Tribological properties of fluorinated Ti48Al2Nb2Cr at elevated temperatures

The friction and wear properties of the fluorinated Ti48Al2Nb2Cr serviced at elevated temperatures are investigated. Figure 6 shows the evolution of the friction coefficients of fluorinated Ti48Al2Nb2Cr when exposed at 200, 400, and 600 °C. The data of the untreated Ti48Al2Nb2Cr were also collected as the control. The friction coefficient of untreated Ti48Al2Nb2Cr remains almost the same (around 0.3) when serviced at 200 and 400 °C. With further increasing the service temperature to 600 °C, the friction coefficient increases to 0.6. For the fluorinated Ti48Al2Nb2Cr, the friction coefficients at 200 and 400 °C fluctuate around 0.4 and 0.9, respectively. This may be due to the uneven surface caused by the adhesive wear. At 600 °C, the friction coefficient reduces to 0.6, similar to that of the untreated specimen.

The topography images of untreated and fluorinated Ti48Al2Nb2Cr at elevated temperatures were collected in Fig. 7. When tested at 200 °C (Figs. 7(a_1, a_2)) and 400 °C (Figs. 7(b_1, b_2)), obvious and deep wear tracks can be found on untreated Ti48Al2Nb2Cr, suggesting the severe wear regime. As displayed in Figs. 7(c_1, c_2), when the service temperature increases to 600 °C, the depth of the wear track becomes shallow but the width of the wear track increases. Additionally, obvious reddish brown component can be found in the wear track (Fig. 7(c_1)), likely caused by the wear and oxidation of the GGr15 counterpart at elevated temperatures. When tested at elevated temperatures, the main wear mechanism of the untreated Ti48Al2Nb2Cr is

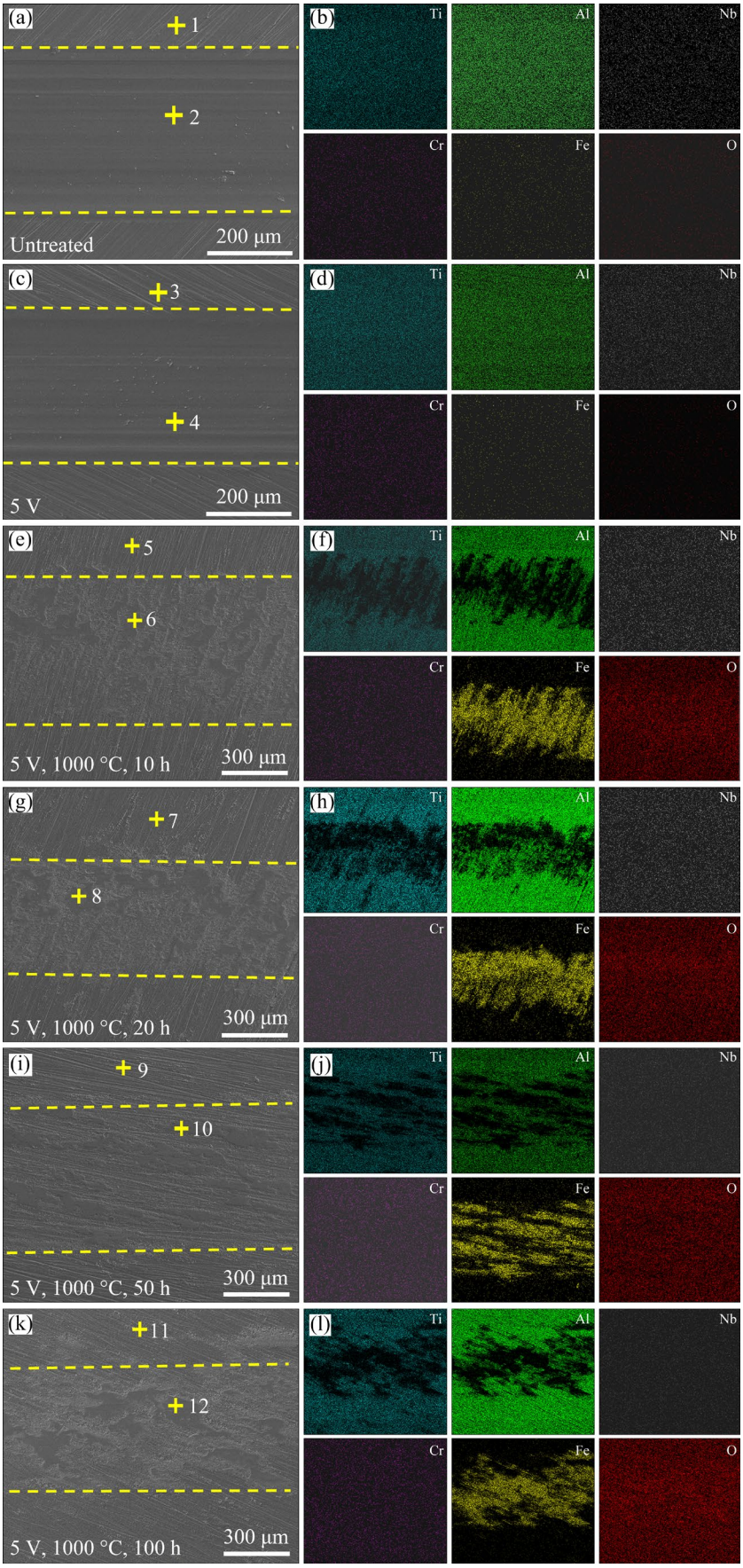

Fig. 4 Top-surface SEM images (a, c, e, g, i, k) and corresponding EDS mappings (b, d, f, h, j, l) of untreated Ti48Al2Nb2Cr (a, b) and fluorinated Ti48Al2Nb2Cr after oxidation at 1000 °C for different time (c−l)

Table 1 EDS results of positions marked in Fig. 4

Point	Content/at.%						
	Ti	Al	Nb	Cr	Fe	O	F
1	59.5	37.3	1.3	1.9	–	–	–
2	50.1	45.9	2.1	1.9	–	–	–
3	48.2	45.5	1.9	2.0	–	–	2.4
4	50.5	45.4	2.0	2.1	–	–	–
5	12.5	20.2	–	0.7	–	66.6	–
6	1.2	0.3	–	0.6	30.4	56.6	–
7	13.3	23.5	–	0.7	–	62.5	–
8	1.2	0.4	–	0.1	30.1	53.3	–
9	11.4	24.6	–	0.4	–	63.6	–
10	2.5	1.5	–	0.45	29.3	66.2	–
11	1.1	32.2	–	0.3	–	66.4	–
12	0.2	1.7	–	0.7	37.3	60.1	–

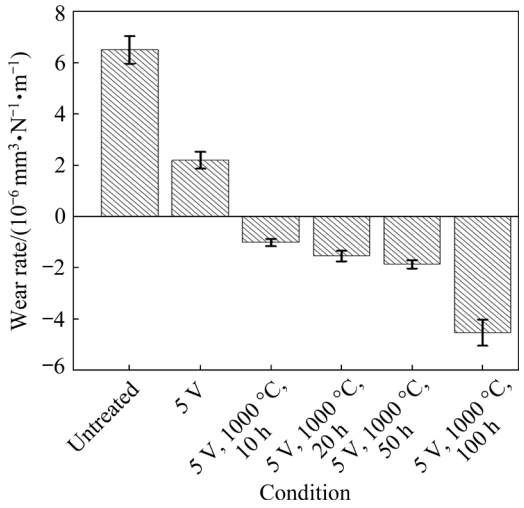

Fig. 5 Wear rates of untreated and fluorinated Ti48Al2Nb2Cr after oxidation at 1000 °C for different time

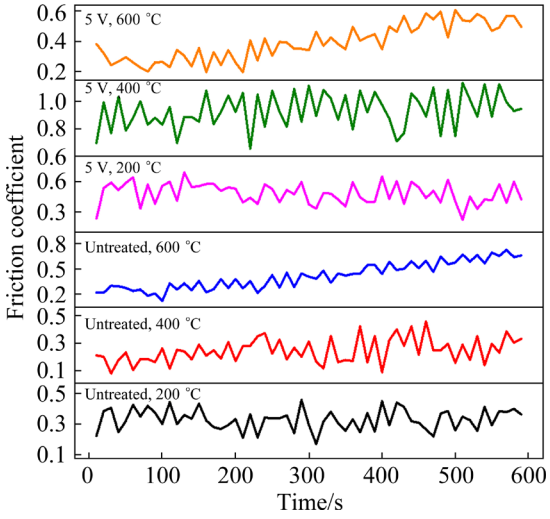

Fig. 6 Evolution of friction coefficients of untreated and fluorinated Ti48Al2Nb2Cr at different temperatures

abrasive wear in the early stage, while adhesive wear and oxidation wear become the main wear mechanism in the following stages.

For the fluorinated Ti48Al2Nb2Cr, the wear tracks generated at different temperatures have similar morphologies (Figs. 7(d_1–f_1, d_2–f_2). Moreover, the 3D topography images indicate that no significant difference can be found on the wear track and unworn region (Figs. 7(d_2, e_2, f_2)). Notably, obvious reddish-brown components can be found in all wear tracks. With a high hardness feature, the Al_2O_3-enriched oxide scale cannot be worn out by the GCr15 counterpart [22]. Combined with the EDS results (Fig. 8), it can be concluded that this reddish-brown component mainly consists of iron oxide derived from the adhesive wear of the GCr15 counterpart. The key difference among these specimens is the width of the wear tracks. In detail, the width of the wear track increases from 930 to 1310 μm when the service temperature increases from 200 to 600 °C (Figs. 7(d_1–f_1, d_2–f_2), implying that the wear resistance of the fluorinated Ti48Al2Nb2Cr is enhanced and wear of the GCr15 counterpart is aggravated at higher temperatures. Similarly, other studies also revealed that the tribological property of TiAl alloy was closely related to the service temperature [19,32,35,36].

For untreated Ti48Al2Nb2Cr, the wear tracks dispersed with some abrasive debris at 200 °C (Fig. 8(a)) and 400 °C (Fig. 8(c)) are relatively smooth. This indicates the abrasion of the untreated Ti48Al2Nb2Cr by the GCr15 counterpart. The EDS results (Points 3 and 6 in Fig. 8 and Table 2) show that the abrasive debris is mainly composed of the mixed oxides of titanium and aluminum, indicating abrasive wear and oxidation wear are the main wear regimes. When the tribological test is carried out at 600 °C (Fig. 8(e)), a wear track with a groove boundary can be found on untreated Ti48Al2Nb2Cr, suggesting the occurrence of abrasive wear. Additionally, a considerable amount of irregular wear debris emerges in the middle of the wear track. Interestingly, the EDS analysis (Point 9 in Fig. 8(e) and Table 2, and Fig. 8(f)) demonstrates that the wear track is rich in Fe and O, indicating the adhesive wear between the Ti48Al2Nb2Cr and GCr15 pairs. Moreover, it is found that the O content in the unworn region in untreated Ti48Al2Nb2Cr increases with the increase of the service temperature (Fig. 8 and Table 2). For the untreated

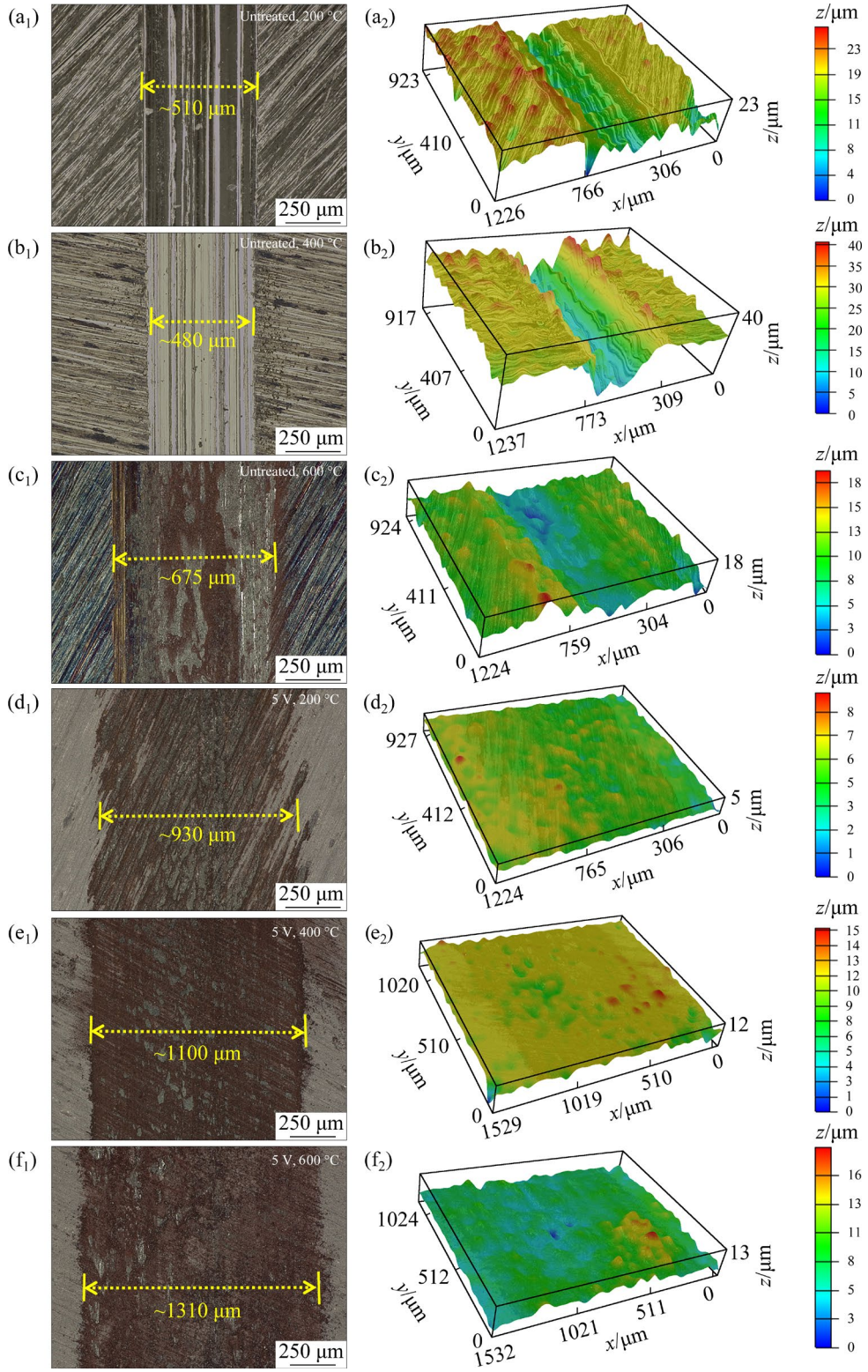

Fig. 7 2D (a_1–f_1) and 3D (a_2–f_2) images of untreated (a_1–c_1, a_2–c_2) and fluorinated (d_1–f_1, d_2–f_2) Ti48Al2Nb2Cr at different service temperatures

Ti48Al2Nb2Cr undergoing the tribological test at 600 °C, the O content on the surface reaches up to 57.2 at.% (Point 7 in Fig. 8(e) and Table 2). Owing to the thermal oxidation and friction-induced heating effect at high service temperatures, a mixture oxide scale consisting of TiO_2 and Al_2O_3 aggravates the abrasive wear between the GCr15 and Ti48Al2Nb2Cr pairs.

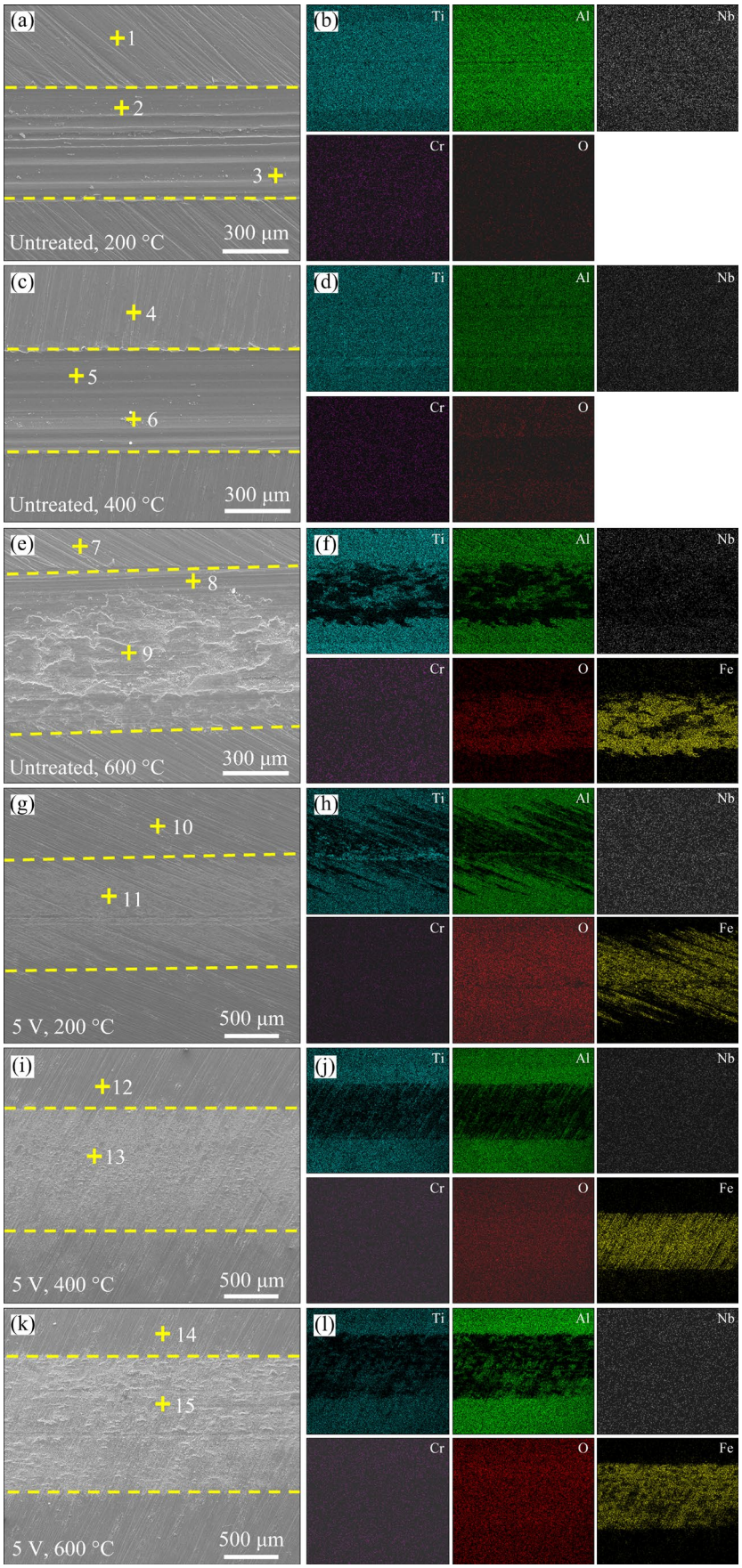

Fig. 8 Top-surface SEM images (a, c, e, g, i, k) and corresponding EDS mappings (b, d, f, h, j, l) of untreated (a−f) and fluorinated (g−l) Ti48Al2Nb2Cr at different service temperatures

Table 2 EDS results of positions marked in Fig. 8

Point	Content/at.%					
	Ti	Al	Nb	Cr	Fe	O
1	48.1	48.2	2.0	1.7	−	−
2	53.0	42.5	2.0	2.5	−	−
3	25.9	26.1	1.0	1.1	−	45.9
4	42.1	36.5	1.6	1.7	−	18.1
5	49.2	46.8	2.3	1.7	−	−
6	17.9	21.00	0.7	0.7	−	59.7
7	21.6	19.4	0.9	0.9	−	57.2
8	42.7	35.2	1.7	2.0	−	18.4
9	2.2	1.5	−	0.4	32.1	63.8
10	12.7	22.9	−	0.5	-	63.9
11	4.2	6.0	−	0.4	23.3	66.1
12	12.9	24.9	−	0.6	−	61.6
13	5.2	8.4	−	0.5	19.7	66.2
14	11.8	21.9	0.1	0.7	−	65.5
15	4.5	7.0	−	0.6	25.2	62.7

For the fluorinated Ti48Al2Nb2Cr, obvious different phenomena can be found (Figs. 8(g−l)). For one thing, even though the tribological tests are conducted at 200 °C (Fig. 8(g)) and 400 °C (Fig. 8(i)), Fe element can be detected in the wear tracks (Figs. 8(h, j)). As mentioned above, for untreated Ti48Al2Nb2Cr obvious Fe element can be identified in the wear track only when the friction and wear test is conducted at 600 °C (Fig. 8(f)). For another, the scratches derived from the sand ground process are still observed in all wear tracks (Figs. 8(g, i, k)), indicating that the oxide scale on the fluorinated Ti48Al2Nb2Cr is not damaged by the GCr15 counterpart. In addition, the grooves observed on the untreated Ti48Al2Nb2Cr (Figs. 8(a, c, e)) disappear on the fluorinated Ti48Al-2Nb2Cr (Figs. 8(g, i, k)). This can be ascribed to the priorly generated oxides on the fluorinated Ti48Al2Nb2Cr.

The wear rate results indicate that elevated temperatures lead to severe abrasion for untreated Ti48Al2Nb2Cr (Fig. 9), evidenced by the nearly doubled wear rate at 400 °C compared with that at 200 °C, followed by a decrease in wear rate when further increasing the temperature to 600 °C. Increasing the service temperature not only promotes the generation of alumina and titania mixture on Ti48Al2Nb2Cr but also causes severe oxidation for the GCr15 counterpart to form iron-based oxide. This leads to severe wear of the GCr15 counterpart. The tribo-film derived from the GCr15 counterpart transfers to the surface of Ti48Al2Nb2Cr and fills in the wear track, resulting in the reduced apparent wear rate. For the fluorinated Ti48Al2Nb2Cr, the wear tracks are even protruding compared to those on the unworn regions independent of the tested temperature (Figs. 8(g, i, k)). This is because the wear debris from the GCr15 counterpart is adherent to the alloy surface during the tribological test. Consequently, the calculated wear rates on these specimens have negative values, indicating excellent wear performance of fluorinated Ti48Al2Nb2Cr at elevated temperatures. Moreover, insignificant difference can be found in the wear rates for the specimens tested at 200 and 400 °C. Whereas, increasing the temperature to 600 °C results in a dramatic difference in the wear rate, suggesting the aggravated deterioration of the GCr15 counterpart and the enhanced stability for the fluorinated Ti48Al2Nb2Cr during the tribological test.

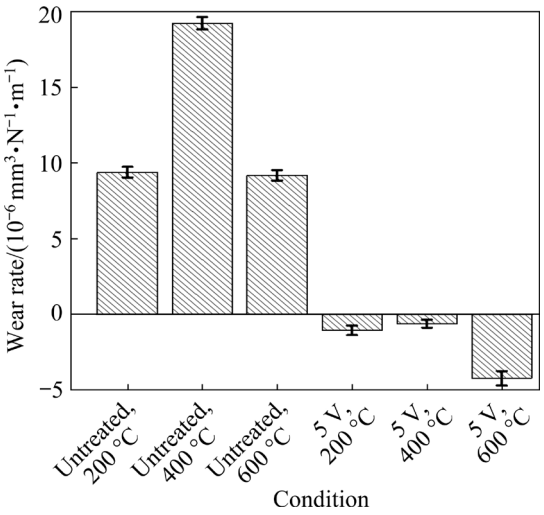

Fig. 9 Wear rates of untreated and fluorinated Ti48Al2Nb2Cr after tribological test at different temperatures

Figure 10 shows the optical images of the wear scars on the GCr15 counterparts after the tribological test with the untreated and fluorinated Ti48Al2Nb2Cr at 25 and 600 °C. Wear scars with similar structures are found regardless of the type of specimens or the service temperatures. Nevertheless, the diameters of the wear scars formed at 25 °C are

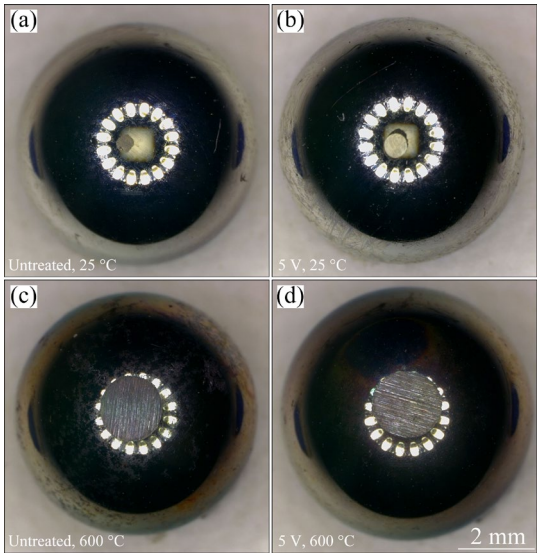

Fig. 10 Wear scars of GCr15 counterpart balls after friction and wear test with untreated (a, c) and fluorinated (b, d) Ti48Al2Nb2Cr at 25 °C (a, b) and 600 °C (c, d)

much smaller than those formed at 600 °C, likely due to the enhanced oxidative wear and adhesive wear for the specimens tested at 600 °C.

After the tribological test at 600 °C, the microstructure and composition of the wear debris were collected and characterized. Both untreated and fluorinated specimens show similar irregular and strip wear debris (Fig. 11). EDS analysis results illustrate that all wear debris are mainly composed of Fe-based oxide (Points 1−3 in Fig. 11 and Table 3), and no Ti, Al, and Nb from the Ti48Al2Nb2Cr matrix can be detected. This indicates that the wear debris originates from the GCr15 counterpart due to adhesion wear and oxidation wear.

3.3 Mechanical properties of fluorinated Ti48Al2Nb2Cr

Consensus has been established that the wear resistance of alloy is in proportion to its surface hardness [37]. Specimens with higher hardness generally exhibit better wear resistance. Figure 12 displays the surface hardness of untreated and fluorinated Ti48Al2Nb2Cr serviced at 1000 °C for different time. The fluorinated Ti48Al2Nb2Cr has slightly higher surface hardness than the untreated Ti48Al2Nb2Cr, which is caused by the formation of

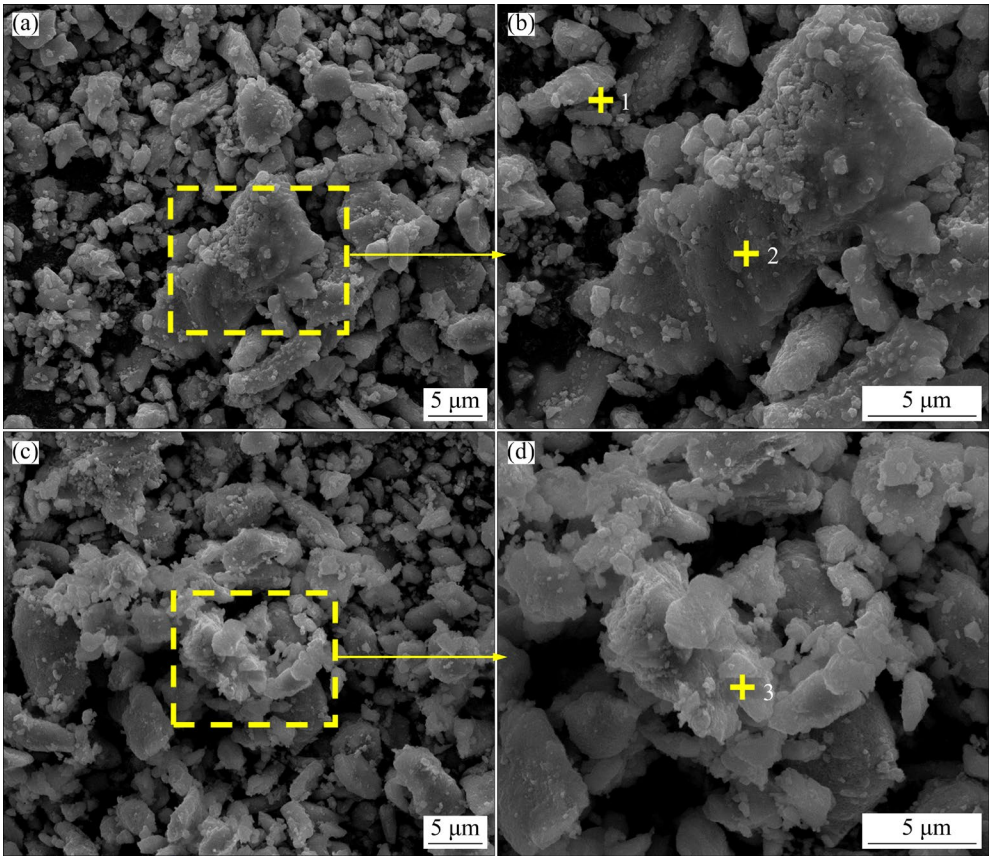

Fig. 11 Top-surface SEM images of wear debris collected from untreated (a, b) and fluorinated (c, d) Ti48Al2Nb2Cr after undergoing tribological test at 600 °C

Table 3 EDS results of positions marked in Fig. 11

Point	Content/at.%			
	Cr	Fe	Mn	O
1	0.7	57.9	0.2	41.2
2	0.9	65.6	0.2	33.3
3	0.7	35.5	0.1	63.7

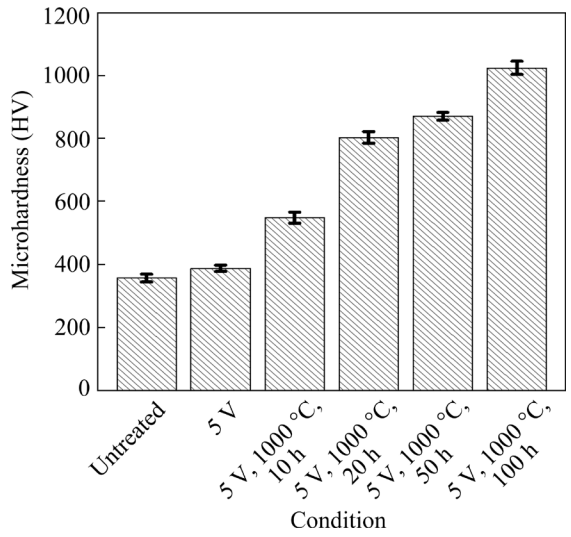

Fig. 12 Vickers hardness of untreated and fluorinated Ti48Al2Nb2Cr after oxidation at 1000 °C for different durations

Al_2O_3-enriched anodic film [11]. When exposed in air at 1000 °C, the aluminum fluorine component in the anodic film converts to Al_2O_3 based oxide scale as a result of the fluorine effect [31]. Moreover, it is found that the Al_2O_3 content in the oxide scale increases with the increase of exposure time (Table 1). Therefore, the hardness of the fluorinated Ti48Al2Nb2Cr shows an upward trend with the prolonging of oxidation time. After oxidation for 100 h, the hardness of the fluorinated Ti48Al2Nb2Cr is more than twice that of the pristine fluorinated Ti48Al2Nb2Cr. This is reflected in the wear resistance of the fluorinated Ti48Al2Nb2Cr which also gradually increases with the increase of exposure time, also confirmed by the morphology of the wear track (Figs. 3 and 4) and wear rate (Fig. 5).

In the present work, a scratch test was performed to evaluate the adhesion between the oxide scale and substrate. During the test, a scratch tip with a conical shape is drawn across the surface of the specimen under the increased load until a certain failure occurs at a certain load, defined as "critical load" [38]. For the fluorinated Ti48Al2Nb2Cr after 10 h oxidization (Fig. 13(a)), a sharp decline of voltage appears at 5.4 N, corresponding to the initial failure of the oxide scale. Prolonging the oxidization time to 20 and 50 h, the critical load values slightly increase to 7.4 and 7.6 N, respectively. This is because the oxide scales on these specimens have similar compositions and are both composed of a mixture of aluminum- and titanium-based oxides (Points 5, 7 and 9 in Fig. 4 and Table 1). Further increasing the load results in a fluctuation in voltage values, indicating the appearance of cracks on the oxide scale. Figure 13(a) also reveals that with prolonging the thermal exposure time, the critical load is gradually postponed, suggesting an improved adhesion between the oxide scale and substrate. It is also worth noting that the specimen with 100 h thermal exposure shows the highest critical load of 13.9 N (Fig. 13(b)), a clear sign of excellent mechanical strength.

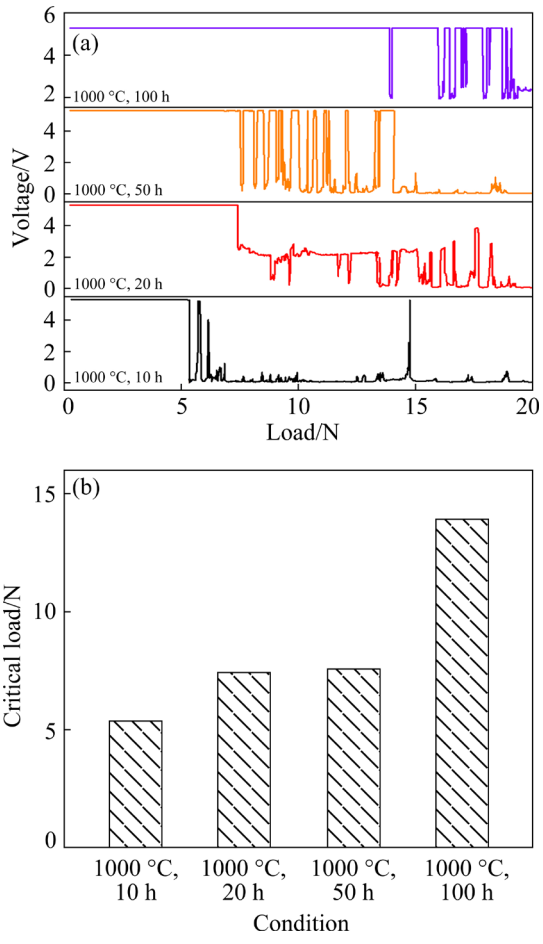

Fig. 13 Voltage−load curves (a) and critical loads (b) of fluorinated Ti48Al2Nb2Cr from scratch test under different conditions

The morphologies of the scratches were characterized by SEM (Fig. 14). As shown in Figs. 14(a) and (b), the oxide scale is damaged by the diamond indenter and results in the edge spalling. Moreover, with increasing the load, gradually widened grooves can be found on the scratches. With lengthening the thermal exposure time to 50 and 100 h, slight edge spalling is found (Figs. 14(c) and (d)). Moreover, the oxide scales remain intact even when the test load reaches 10 N, indicating good adhesion with the substrate and stability against external force.

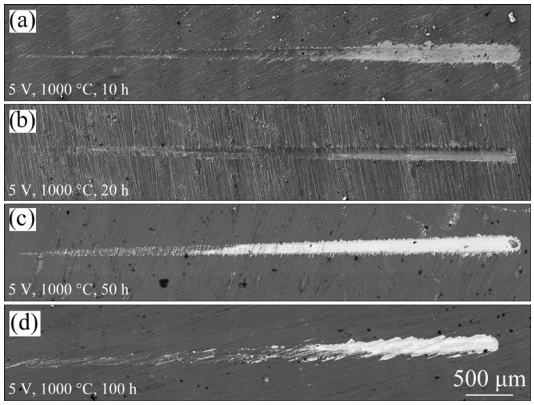

Fig. 14 SEM images of scratches derived from fluorinated Ti48Al2Nb2Cr after oxidation at 1000 °C for 10 h (a), 20 h (b), 50 h (c), and 100 h (d)

4 Conclusions

(1) Anodic fluorination has a marginal influence on the friction coefficient, as well as the friction and wear properties of Ti48Al2Nb2Cr at 25 °C. Both untreated and fluorinated Ti48Al2Nb2Cr specimens exhibit poor wear resistance. The wear process is dominated by abrasive wear and oxidation wear.

(2) The friction and wear properties of the untreated Ti48Al2Nb2Cr decrease with increasing service temperature. Abrasive wear is the main wear mechanism in the early stage, while adhesive wear and oxidation wear become the main wear mechanism in the following stages.

(3) Exposure in air at high temperatures promotes the formation of Al_2O_3-enriched oxide scale on the fluorinated Ti48Al2Nb2Cr owing to the fluorine effect, significantly improves the adhesion strength between the oxide scale and alloy substrate, as well as enhances surface hardness and wear resistance. Oxidation wear and adhesion wear are the dominant wear mechanisms for the fluorinated Ti48Al2Nb2Cr alloy.

CRediT authorship contribution statement

Ji-jian GUO: Data curation, Writing − Original draft preparation; **Zhe-xuan LI:** Investigation, Data curation, Writing − Original draft preparation; **Qing-qing SUN:** Writing − Reviewing and editing; **Lian-kui WU:** Supervision, Conceptualization, Data curation, Funding acquisition, Writing − Reviewing and editing; **Fa-he CAO:** Writing − Reviewing and editing.

Declaration of competing interest

The authors declare that they have no known competing financial interests or personal relationships that could have appeared to influence the work reported in this paper.

Acknowledgments

This work was financially supported by the National Natural Science Foundation of China (No. 52271084), the Guangdong Basic and Applied Basic Research Foundation, China (No. 2021B1515020056), and the Open Research Fund of Songshan Lake Materials Laboratory, China (No. 2022SLABFK06). Also, the authors would like to thank Dr. Guang-xi DONG for English language editing.

References

[1] WU Lian-kui, WU Jing-jia, WU Wei-yao, CAO Fa-he, JIANG Mei-yan. Sol–gel-based coatings for oxidation protection of TiAl alloys [J]. Journal of Materials Science, 2020, 55(15): 6330−6351.

[2] GAO Qiang, ZHANG Lai-qi, QIAO Yi, LIN Jun-pin. Diffusion bonding behaviour of β−γ TiAl alloys containing high niobium with Ti interlayer by spark plasma sintering [J]. Transactions of Nonferrous Metals Society of China, 2022, 32(12): 3973−3984.

[3] ZHAO Peng-xiang, LI Xiao-bing, XING Wei-wei, CHEN Bo, MA Ying-che, LIU Kui. Cyclic oxidation behavior of Nb/Mn/Si alloying beta−gamma TiAl alloys [J]. Transactions of Nonferrous Metals Society of China, 2023, 33(1): 128−140.

[4] MENG Bo, WANG Jin-long, CHEN Ming-hui, ZHU Sheng-long, WANG Fu-hui. Study on the oxidation behavior of a novel thermal barrier coating system using the nanocrystalline coating as bonding coating on the single-crystal superalloy [J]. Corrosion Science, 2023, 225: 111591.

[5] JIANG Min-jin, SUN Hong-liang, LIU Rui, JIANG Xiao-song, ZHANG Ya-li, SUN Da-ming. Fabrication and mechanical properties of Ti_2AlN/TiAl composite with continuous network structure [J]. Transactions of Nonferrous

Metals Society of China, 2023, 33(5): 1437−1451.
[6] PFLUMM R, FRIEDLE S, SCHÜETZE M. Oxidation protection of γ-TiAl-based alloys — A review [J]. Intermetallics, 2015, 56: 1−14.
[7] DUAN Bao-hua, YANG Yu-chen, HE Shi-yu, FENG Qi-sheng, MAO Lu, ZHANG Xue-xian, JIAO Li-na, LU Xiong-gang, CHEN Guang-yao, LI Chong-he. History and development of γ-TiAl alloys and the effect of alloying elements on their phase transformations [J]. Journal of Alloys and Compounds, 2022, 909: 164811.
[8] SUN Tie-long, GUO Zhi-chao, CAO Jun, LIANG Yong-feng, LIN Jun-pin. Isothermal oxidation behavior of high-Nb-containing TiAl alloys doped with W, B, Y, and C/Si [J]. Corrosion Science, 2023, 213: 110980.
[9] PANOV D O, SOKOLOVSKY V S, STEPANOV N D, ZHEREBTSOV S V, PANIN P V, NOCHOVNAYA N A, SALISHCHEV G A. Oxidation resistance and thermal stability of a β-solidified γ-TiAl based alloy after nitrogen ion implantation [J]. Corrosion Science, 2020, 177: 109003.
[10] WU Lian-kui, XIA Jun-jie, JIANG Mei-yan, WANG Qi, WU Hai-xin, SUN Dong-bai, YU Hong-ying, CAO Fa-he. Oxidation behavior of Ti45Al8.5Nb alloy anodized in NH_4F containing solution [J]. Corrosion Science, 2020, 166: 108447.
[11] LI Zhe-xuan, YAN Hao-jie, LI Xin-ran, MENG Xian-ze, LIU Ren-ci, JIA Qing, WU Lian-kui, CAO Fa-he. The long-term isothermal oxidation and cyclic oxidation performance of anodized Ti48Al2Nb2Cr alloy [J]. Corrosion Science, 2022, 199: 110200.
[12] XU Chi, ZHU Ming-hao, GAO Chuan-li, GUAN Hao-hao, WANG Xing-ping, JIN Xiao-yue, DU Jian-cheng, XUE Wen-bin. Microstructural characterizations of γ-TiAl alloy after high-temperature steam oxidations at 900, 1000, 1100 and 1200 °C [J]. Materials Characterization, 2022, 189: 111979.
[13] SWADŹBA R, BAUER P P. Microstructure formation and high temperature oxidation behavior of Ti−Al−Cr−Y−Si coatings on TiAl [J]. Applied Surface Science, 2021, 562: 150191.
[14] WU Jing-jia, YAN Hao-jie, CAO Fa-he, WU Lian-kui. The oxidation performance and interfacial reaction behavior of YSZ-ZrB_2 incorporated glass composite coating [J]. Corrosion Science, 2021, 189: 109622.
[15] WU Jing-jia, YAN Hao-jie, CAO Fa-he, WU Lian-kui. Oxidation performance and interfacial reaction behavior of glass-ceramic coating on TiAl alloy with electrodeposited SiO_2 interlayer [J]. Surface and Coatings Technology, 2021, 422: 127495.
[16] ZHANG Kai, XIN Li, MA Tian-yu, CHANG Hao, LU Yi-liang, FENG Chang-jie, ZHU Sheng-long, WANG Fu-hui. Investigation of the role of silicon in TiAlSiN coating deposited on TiAl alloys during long-term oxidation [J]. Corrosion Science, 2022, 204: 110394.
[17] MIYOSHI K, LERCH B A, DRAPER S L. Fretting wear of Ti−48Al−2Cr−2Nb [J]. Tribology International, 2003, 36 (2): 145−153.
[18] LI Chen-xi, XIA Jing, DONG Han-shan. Sliding wear of TiAl intermetallics against steel and ceramics of Al_2O_3, Si_3N_4 and WC/Co [J]. Wear, 2006, 261(5): 693−701.
[19] MENGIS L, GRIMME C, GALETZ M C. High-temperature sliding wear behavior of an intermetallic γ-based TiAl alloy [J]. Wear, 2019, 426/427: 341−347.
[20] GARCÍA-MARTÍNEZ E, MIGUEL V, MARTÍNEZ A, NARANJO J A, COELLO J. Tribological characterization of tribosystem Ti48Al2Cr2Nb-coated/uncoated carbide tools at different temperatures [J]. Wear, 2021, 484/485: 203992.
[21] HUA Ke, WAN Qiong, TONG Yan-lin, YANG Guang, WU Hong-xing, ZHOU Qing, WANG Hai-feng. Microstructural feature dependence of dry sliding wear behaviors in a γ-TiAl alloy [J]. Wear, 2021, 484/485: 204039.
[22] LI Zhe-xuan, BAO Ya-ting, WU Lian-kui, CAO Fa-he. Oxidation and tribological properties of anodized Ti45Al8.5Nb alloy [J]. Transactions of Nonferrous Metals Society of China, 2021, 31(11): 3439−3451.
[23] WU Feng-he, ZHANG Ning, SUN Ying-bing, LI Xiang, LIU Zi-jian, YANG Yu-lin. Effect of applied load on tribological behaviour of Ti−48Al−2Cr−2Nb alloy under oil-lubricated condition [J]. Wear, 2024, 538/539: 205210.
[24] RASTKAR A R, BELL T. Characterization and tribological performance of oxide layers on a gamma based titanium aluminide [J]. Wear, 2005, 258(11/12): 1616−1624.
[25] SOPUNNA K, THONGTEM T, MCNALLAN M, THONGTEM S. Formation of titanium nitride on γ-TiAl alloys by direct metal−gas reaction [J]. Journal of Materials Science, 2006, 41: 4654−4662.
[26] LIU Xiao-ping, TIAN Wen-huai, XU Wei, LIANG Wen-ping, XU Zong. Wear resistance of TiAl intermetallics by plasma alloying and plasma carburization [J]. Surface and Coatings Technology, 2007, 201(9): 5278−5281.
[27] LI Jia-ning, CHEN Chuan-zhong, SQUARTINI T, HE Qing-shan. A study on wear resistance and microcrack of the Ti_3Al/TiAl+TiC ceramic layer deposited by laser cladding on Ti−6Al−4V alloy [J]. Applied Surface Science, 2010, 257(5): 1550−1555.
[28] WU Xiang-qing, XIE Fa-qin, HU Zong-chun, WANG Li. Effects of additives on corrosion and wear resistance of micro-arc oxidation coatings on TiAl alloy [J]. Transactions of Nonferrous Metals Society of China, 2010, 20(6): 1032−1036.
[29] LI Feng-kun, RAWAT R S, ZHANG Ping-ze, WEI Dong-bo, YANG Ka, DANG Bo. Mechanical properties and reciprocating sliding tribological behaviors of γ-TiAl substrate and plasma-based Mo−Si−Ti coating [J]. Journal of Materials Research and Technology, 2023, 26: 1469−1483.
[30] YAN Hao-jie, XIA Jun-jie, WU Lian-kui, CAO Fa-he. Hot corrosion behavior of Ti45Al8.5Nb alloy: Effect of anodization and pre-oxidation [J]. Acta Metallurgica Sinica (English Letters), 2022, 35(9): 1531−1546.
[31] DONCHEV A, MENGIS L, COURET A, MAYER S, CLEMENS H, GALETZ M. Effects of tungsten alloying and fluorination on the oxidation behavior of intermetallic titanium aluminides for aerospace applications [J]. Intermetallics, 2021, 139: 107270.
[32] MENGIS L, GRIMME C, GALETZ M C. Tribological properties of the uncoated and aluminized Ti−48Al−2Cr−2Nb TiAl alloy at high temperatures [J]. Wear, 2021, 477: 203818.
[33] WANG H W, SKELDON P, THOMPSON G E. Development

and tribological assessment of self-lubricating anodic films on aluminium [J]. Surface and Coatings Technology, 1997, 88(1/2/3): 269−273.

[34] LEE G S, CHOI J H, CHOI Y C, BU S D, LEE Y Z. Tribological effects of pores on an anodized Al alloy surface as lubricant reservoir [J]. Current Applied Physics, 2011, 11(Supplement): 182−186.

[35] CHENG Jun, YANG Jun, ZHANG Xing-hua, ZHONG Hong, MA Ji-qiang, LI Fei, FU Li-cai, BI Qin-ling, LI Jin-shan, LIU Wei-min. High temperature tribological behavior of a Ti−46Al−2Cr−2Nb intermetallics [J]. Intermetallics, 2012, 31: 120−126.

[36] CHENG Fang, LIN Jun-pin, LIANG Yong-feng. Friction and wear properties of a high Nb-containing TiAl alloy against WC-8Co, Si_3N_4, and GCr_{15} in an unlubricated contact [J]. Intermetallics, 2019, 106: 7−12.

[37] ZHAI Wen-zheng, BAI Li-chun, ZHOU Run-hua, FAN Xue-ling, KANG Guo-zheng, LIU Yong, ZHOU Kun. Recent progress on wear-resistant materials: Designs, properties, and applications [J]. Advanced Science, 2021, 8(11): e2003739.

[38] ABEGUNDE O O, MAKHA M, MACHKIH K, LARHLIMI H, GHAILANE A, SAMIH Y, ALAMI J. Structural, mechanical and corrosion resistance of phosphorus-doped TiAlN thin film [J]. Journal of Materials Science, 2022, 57(40): 19107−19130.

氟化处理 Ti48Al2Nb2Cr 合金的摩擦磨损性能

郭积坚，李哲轩，孙擎擎，伍廉奎，曹发和

中山大学 材料学院，深圳 518107

摘　要：在含 NH_4F 的电解液中对 Ti48Al2Nb2Cr(摩尔分数，%)合金进行阳极氟化处理以提高合金在室温和高温下的摩擦磨损性能。考察了氟化处理对 Ti48Al2Nb2Cr 合金摩擦因数、磨损率、磨痕形貌以及氧化膜与基体结合强度的影响。结果表明，在空气氧化过程中，由于氟效应促进了 Ti48Al2Nb2Cr 合金表面原位形成富含 Al_2O_3 的氧化膜，合金表面硬度和耐磨性能都得到了提高。经摩擦磨损实验后，经阳极氟化处理后的 Ti48Al2Nb2Cr 合金表面无明显变化，而 GCr15 对磨副磨损严重，表明阳极氟化处理可显著改善 Ti48Al2Nb2Cr 合金的摩擦磨损性能。氟化处理 Ti48Al2Nb2Cr/GCr15 对磨副在高温下的磨损机制主要为氧化磨损和黏着磨损。

关键词：TiAl 合金；阳极氟化；氟化效应；摩擦学性能；耐磨性能

(Edited by Wei-ping CHEN)